Original Article

JCBFM

Journal of Cerebral Blood Flow & Metabolism
2018, Vol. 38(7) 1213–1226

DOI: 10.1177/0271678X17709463
journals.sagepub.com/home/jcbfm
SAGE

Increased astroglial activity and reduced neuronal function across brain in AβPP-PS1 mouse model of Alzheimer's disease

Anant B Patel, Vivek Tiwari, Pandichelvam Veeraiah and Kamal Saba

Abstract

Alzheimer's disease (AD) is the most common neurodegenerative disease associated with progressive loss of cognitive function, personality, and behavior. The present study evaluates neuronal and astroglial metabolic activity, and neurotransmitter cycle fluxes in AβPP-PS1 mouse model of AD by using ^{1}H-[^{13}C]-nuclear magnetic resonance (NMR) spectroscopy together with an infusion of either [1,6-$^{13}C_2$]glucose or [2-^{13}C]acetate. The levels of *N*-acetyl-aspartate (NAA) and glutamate were found to be decreased in the cerebral cortex and hippocampus in AβPP-PS1 mice, when compared with wild type controls. The cerebral metabolic rate of acetate oxidation was increased in the hippocampus and cerebral cortex of AβPP-PS1 mice suggesting enhanced astroglial activity in AD. AβPP-PS1 mice exhibit severe reduction in glutamatergic and gamma-amino butyric acid (GABA)ergic neuronal metabolic activity and neurotransmitter cycling fluxes in the hippocampus, cerebral cortex, and striatum as compared with controls. These data suggest that metabolic activity of excitatory and inhibitory neurons is compromised across brain in AβPP-PS1 mouse model of AD.

Keywords

Gamma-amino butyric acid, glutamate, ^{13}C nuclear magnetic resonance spectroscopy, neurodegeneration, neuronal–glial interaction

Received 22 November 2016; Revised 24 March 2017; Accepted 19 April 2017

Introduction

Alzheimer's disease (AD) is the most common neurodegenerative disorder associated with gradual deterioration of cognitive functions, personality and memory.[1] The cause and pathogenesis of the disease remains complex but has been shown to be associated with gray matter atrophy, disruption of neuronal function, and formation of neurofibrillary tangles and neuritic plaques in the medial temporal limbic regions and isocortex.[2] The degradation of amyloid precursor protein (AβPP) is central to the pathological cascade that eventually leads to AD.[3] Deficits in numerous neurotransmitters are suggested to build up with progression of the disease.[3]

Quantitative analyses have suggested loss of 25-35% synapses in the postmortem cortical tissue of AD patients.[4] Several positron emission tomography studies have shown glucose hypo-metabolism across brain under mild cognitive impairment and in late onset AD patients.[5] The reduced rates of neuronal glucose oxidation was also shown at an early age in AβPP-presenilin (PS1) mouse model of AD.[6] Glutamate and gamma-amino butyric acid (GABA) are the major excitatory and inhibitory neurotransmitters, respectively, in the mature central nervous system.[7] Majority of brain energy is utilized to sustain the processes associated with these neurotransmitters, which are involved in behavior, cognition, emotion and

CSIR-Centre for Cellular and Molecular Biology, Hyderabad, India

Corresponding author:
Anant B Patel, NMR Microimaging and Spectroscopy, Centre for Cellular and Molecular Biology, Uppal Road, Habsiguda, Hyderabad 500 007, India.
Email: abpatel@ccmb.res.in

memory.[8] Neurons and astroglia work in coordination for the trafficking of neurotransmitters, commonly known as glutamate-glutamine and GABA-glutamine neurotransmitter cycling, to maintain normal functioning of brain. It has been established that rates of neurotransmitter cycling and neuronal glucose oxidation are stochiometrically coupled.[9,10] Moreover, the oxidative glucose metabolism and neurotransmitter cycle rates are shown to increase with brain activity. In vivo ^{13}C nuclear magnetic resonance (NMR) spectroscopy and functional magnetic resonance imaging measurements have established relationships between neurometabolism and neuronal activity that provide novel insights into the nature of brain function.[11] Therefore, neuronal glucose oxidation and neurotransmitter cycling are of prime importance for understanding brain activity and cognitive function. The perturbation in neuronal activity in AD is expected to affect neurotransmitter cycling and metabolic activity of neurons. Hence, a comprehensive understanding of neuronal and astroglial metabolic activities in AD condition is expected to provide better insight about the AD pathology.

AβPP-PS1 mice have been developed by inserting mutants of APP and presenilin at a single locus under the control of mouse prion promoter.[12] These mice exhibit memory impairment and severe amyloid plaque loading, a hall mark of AD, in the cerebral cortex and hippocampus at the age of 12 months. The present study assessed the neuronal and astroglial metabolic activity, and neurotransmitter cycling in AβPP-PS1 mice at the age of 12 months by using ^{1}H-[^{13}C]-NMR spectroscopy in conjunction with infusion of [1,6-$^{13}C_2$]glucose or [2-^{13}C]acetate. Our results indicate compromised neuronal metabolic activity, and enhanced astroglial activity in AD condition.

Materials and methods

All the experimental procedures with mice were approved by the Institutional Animals Ethics Committee of Centre for Cellular and Molecular Biology (CCMB), Hyderabad, India, and were conducted in accordance with the guidelines established by Committee for the Purpose of Control and Supervision on Experiments on Animals, Ministry of Environment and Forests, Government of India. ARRIVE guidelines were followed in the preparation of the manuscript. In order to get rid of the complication of hormonal cycling on the neurometabolism, only male mice has been used. Male AβPP-PS1 ($n = 23$) mice and wild-type littermates ($n = 24$) of age 12 months as confirmed by genotyping for the presence and absence of mutant AβPP and PS1 genes were used for the study.

Assessment of learning and memory in AβPP-PS1 mouse

Learning and memory of mice were evaluated using Morris Water Maze (MWM) test.[13] MWM consists of a circular tank with height and diameter, 50 and 150 cm, respectively, and virtually divided into four equal quadrants with different clues provided on the wall for spatial map of the pool. The pool was filled with water to a depth of 30 cm, and an escape platform (10 cm in diameter) was submerged 0.5 cm under water level in the fourth quadrant. During the training period, mice were left in each quadrant for 90 s to explore the maize. The movement path of mice was video recorded and analyzed by the Ethovision software. Following this period, animals were guided towards the hidden platform that was placed in the fourth quadrant. The training was continued for four days from each quadrants. The memory was assessed on 7 and 8 day with and without the platform. The escape latency to reach the platform, and frequency of crossing over the platform zone were measured.

Infusion of [1,6-$^{13}C_2$]glucose and [2-^{13}C]acetate

Metabolic study was carried out in overnight fasted mice. Animals were anesthetized with urethane (1.5 g/kg, i.p.), and the lateral tail vein was cannulated for administration of ^{13}C labeled substrates. Urethane produces a long-lasting steady level of anesthesia with physiologic and pharmacologic behaviors similar to those observed in unanesthetized condition. The body temperature of animals was maintained at 37°C. [1,6-$^{13}C_2$]Glucose was administered for 10, 30, 60 and 90 min in mice using bolus variable infusion rate protocol.[14] A bolus of 590 μmol/kg of labeled glucose (0.225 mol/L, dissolved in water) was administered in 15 s, there after the infusion rate was stepped down exponentially by decreasing the rate every 30 s. The infusion rate of [1,6-$^{13}C_2$]glucose at steady state (≥8.25 min) was 15 μmol/kg/min. At least four mice were used for each time point. In addition, mice were also infused with [2-^{13}C]acetate + glucose for 15 min (WT, $n = 6$; AβPP-PS1, $n = 5$) and 90 min (WT, $n = 4$; AβPP-PS1, $n = 4$) to evaluate the astroglial metabolic activity and $V_{cyc}/V_{tca(n)}$, respectively. The [2-^{13}C]acetate (1 mol/L) was dissolved in water and pH adjusted to 7.0 using HCl. Initially, [2-^{13}C]acetate was administered a bolus of 1.25 mmol/kg in 15 s. The acetate infusion rate was stepped down every 4 min, and the infusion rate at steady state (≥8 min) was maintained to 0.2 mmol/kg/min.[15] Blood was collected from the retro-orbital sinus artery during the last minute of the experiment, and centrifuged to separate plasma. Blood plasma was stored at −80°C for further analysis.

At the end of the experiment, animal head was frozen *in situ* using liquid nitrogen.

Preparation of brain extracts

Frozen brain was chiseled out and dissected in a cryostat maintained at −20°C to isolate the cerebral cortex, hippocampus, and striatum based on mouse brain atlas. The cortical region was separated as the outermost layer after removing the skull, and striatal region was identified as the sub-cortical structure posterior to the prefrontal region. Hippocampus appears as a wing-like structure, with completely different tissue contrast than neighboring tissues, is well distinguished, and easily dissected. Metabolites were extracted from frozen tissue as described previously.[16] The frozen weighed tissues were ground with 0.1 N HCl in methanol (1:2 w/v) in a dry ice/ethanol bath. [2-^{13}C]Glycine was added as an internal concentration reference. [2-^{13}C]Glycine has been used as a concentration reference in several studies.[14,15,17] The tissue powder was homogenized with ethanol, and clarified by centrifugation at 20,000 *g*. The tissue extracts were passed through Chelex column (Biorad), and pH adjusted to 7.0. The lyophilized extracts were dissolved in deuterium oxide containing sodium 3-trimethylsilyl[2,2,3,3-D4]-propionate (TSP) as a chemical shift reference.

Preparation and NMR analysis of blood plasma

Blood plasma was mixed with sodium phosphate buffer, which was prepared in deuterium oxide containing formate, and filtered using a 10-kD cut off centrifugal filter to remove macromolecules. The concentrations and fractional ^{13}C enrichments of glucose and acetate were measured in ^{1}H NMR spectrum of plasma using formate as an internal reference. The percent ^{13}C labeling of glucose-C1α (5.2 ppm) and acetate-C2 (1.9 ppm) was calculated by dividing the intensity of the ^{13}C with the total (^{12}C + ^{13}C).

NMR analysis of brain extract

^{1}H-[^{13}C]-NMR spectra of brain tissue extracts were recorded at 600 MHz NMR spectrometer (Bruker Biospin, Germany).[18] The concentrations of metabolites were determined relative to [2-^{13}C]glycine. The ^{13}C atom percentage enrichment of various metabolites at different carbon positions was determined as the ratio of the peak areas in the ^{1}H-[^{13}C]-NMR difference spectrum (2 × ^{13}C only) to the non-edited spectrum (^{12}C + ^{13}C), and was corrected for the natural abundance (1.1%).

Determination of acetate oxidation

Acetate is transported specifically into astrocytes by monocarboxylate transporters[19] and oxidized therein.[15] Oxidation of [2-^{13}C]acetate in astrocytes labels astroglial glutamine$_{C4}$, which in turn transfers ^{13}C label into glutamate$_{C4}$ and GABA$_{C2}$ via corresponding neurotransmitter cycling.[15] The cerebral metabolic rate of acetate oxidation ($CMR_{Ac(Ox)}$) was calculated as

$$CMR_{Ac(Ox)} = (1/t) \times \left\{[Gln] \times (Gln_{C4}) + fGlu_A \times [Glu] \times \left(Glu_{C4(g)}\right)\right\} \quad (1)$$

where [Gln] and [Glu] are the concentration of glutamine and glutamate, respectively, while Gln_{C4} refers the ^{13}C fractional enrichment of glutamine. $Glu_{C4(g)}$ represents fractional enrichment of astroglial glutamate-C4, and was assumed to be same as the enrichment of glutamine-C4. '$fGlu_A$', represents the fraction of glutamate in astroglia.[14,17]

Determination of V_{cyc}/V_{TCA} from steady state [2-^{13}C]acetate experiment

Steady state ^{13}C labeling of amino acids from [2-^{13}C]acetate was used to determine the ratios, $V_{cyc}/V_{TCA(n)}$ for glutamatergic and GABAergic neurons as described earlier in detail.[14,17] The ratio $V_{cyc(Glu\text{-}Gln)}/V_{TCA(Glu)}$ was calculated as follows

$$\frac{V_{cyc(Glu-Gln)}}{V_{TCA(Glu)}} = \frac{Glu_{C4}}{Gln_{C4} - Glu_{C4}} \quad (2)$$

where Gln_{C4} and Glu_{C4} are the steady state labeling of astroglial glutamine-C4 and neuronal glutamate-C4, respectively. The ^{13}C labeling of Glu_{C4} and Gln_{C4} from [1-^{13}C]/[6-^{13}C]glucose that was formed from [2-^{13}C]acetate was corrected by subtracting [3-^{13}C]lactate labeling.

The ratio $V_{cyc(GABA\text{-}Gln)}/V_{TCA(GABA)}$ was determined as follows

$$\frac{V_{cyc(GABA-Gln)}}{V_{TCA(GABA)}} = \frac{GABA_{C2}}{Gln_{C4} - GABA_{C2}} \quad (3)$$

where $GABA_{C2}$ is the steady state ^{13}C enrichments of [2-^{13}C]GABA from [2-^{13}C]acetate.

Determination of metabolic rates

The ^{13}C labeling of brain amino acids from [1,6-$^{13}C_2$]glucose was used to generate ^{13}C turnover curve of amino acids. A three compartment metabolic model (Figure 1) was fitted to ^{13}C turnover curves to

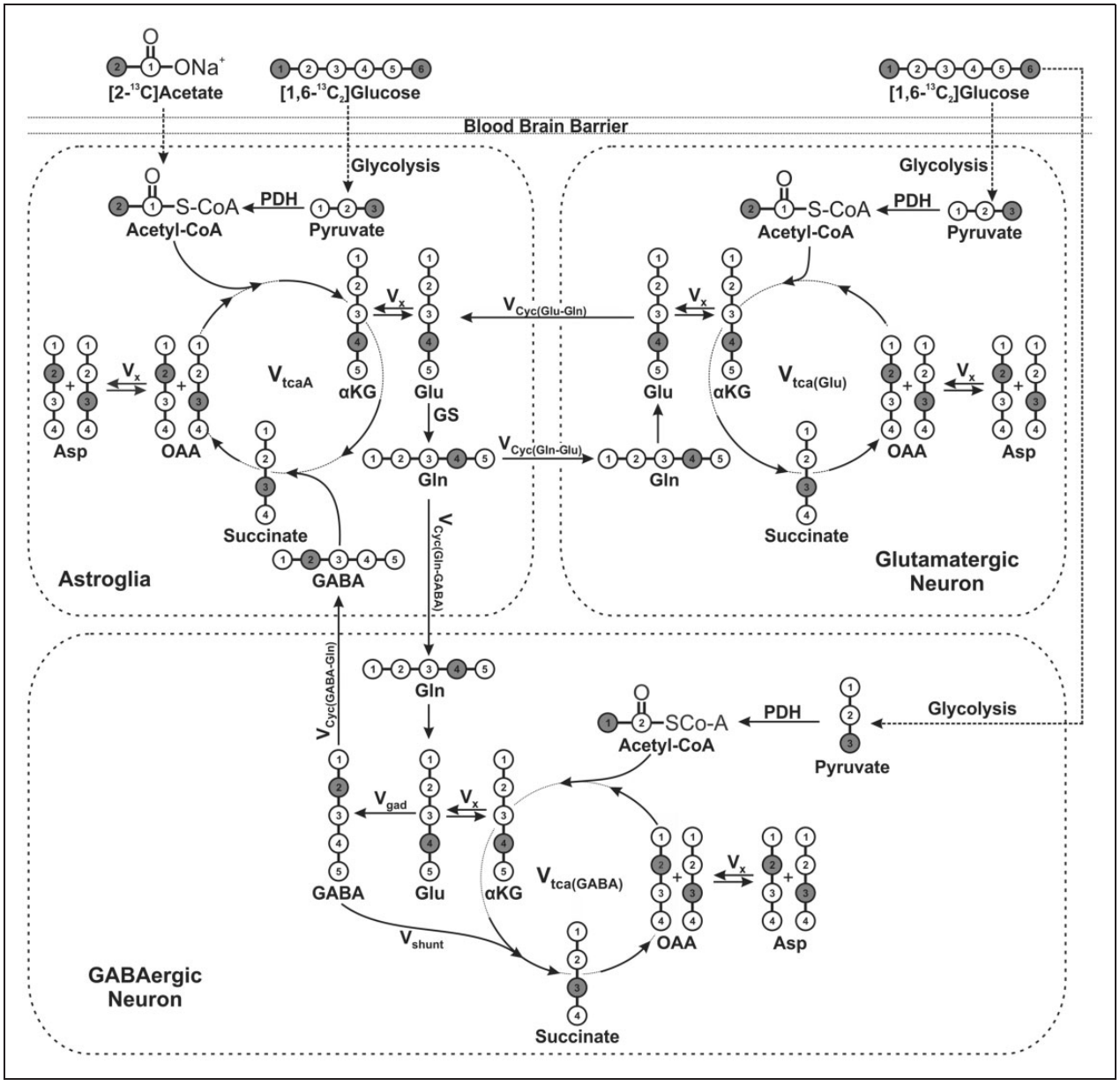

Figure 1. A three compartment metabolic model depicting the ^{13}C labeling of brain metabolites from [1,6-$^{13}C_2$]glucose and [2-^{13}C]acetate.[17] Metabolism of [1,6-$^{13}C_2$]glucose via neuronal TCA cycle labels Glu_{C4}, which is converted to $GABA_{C2}$ by enzyme GAD in GABAergic neurons. Labeling of Gln_{C4} occurs from Glu_{C4} and $GABA_{C2}$ via glutamate–glutamine and GABA–glutamine cycle, respectively. [2-^{13}C]Acetate is selectively transported and metabolized in astroglia and labels Gln_{C4}. Neuronal Glu_{C4} and $GABA_{C2}$ are labeled from Gln_{C4} via glutamine-glutamate and glutamine-GABA cycling, respectively. α-KG: α-ketoglutarate; OAA: oxaloacetate; Asp: aspartate; GABA: γ-aminobutyric acid; Glu: glutamate; GAD: glutamate decarboxylase; Gln: glutamine; $V_{cyc(GABA\text{-}Gln)}$: GABA-glutamine cycling flux; $V_{cyc(Glu\text{-}Gln)}$: glutamate-glutamine cycling flux; V_{gad}: glutamate decarboxylase flux; V_{gln}: glutamine synthesis rate; V_{shunt}: flux of GABA shunt; $V_{tca(A)}$: astroglial TCA cycle flux; $V_{tca(GABA)}$: GABAergic TCA cycle flux; $V_{tca(Glu)}$: glutamatergic TCA cycle flux; V_x: exchange rate between α-ketoglutarate and glutamate. The filled circle represents the position of ^{13}C carbon.

determine metabolic rates.[17] The metabolic model is based on series of mass and ^{13}C isotope balance equations describing ^{13}C labeling of brain metabolites from [1,6-$^{13}C_2$]glucose into neurons and astroglia[14,17] using a CWave software package running in Matlab.[20] The measured concentrations of aspartate, GABA, glutamate, and glutamine in brain tissue were used for metabolic modeling (Table S1). The glutamate pool was divided among GABAergic neurons (2%), astroglia (16%), and glutamatergic neurons (82%).[14] Aspartate was distributed into astroglia, GABAergic neurons, and glutamatergic neurons in the proportion

16:42:42. The GABA and glutamine were assumed to be localized into GABAergic neurons and astrocytes, respectively. The ratios, $V_{cyc(Glu\text{-}Gln)}/V_{TCA(Glu)}$ and $V_{cyc(GABA\text{-}Gln)}/V_{TCA(GABA)}$ (Table 1) obtained from the steady state measurements from [2-^{13}C]acetate were used as constraints during fitting of the model to ^{13}C turnover curve of cerebral amino acids from [1,6-$^{13}C_2$]glucose. The Runge-Kutta algorithm was used to solve the differential equations, and the fitting was carried out using a Levenberg-Marquardt algorithm.[21] The cerebral metabolic rates were determined from the best fit of the metabolic model to the ^{13}C turnover curves of amino acids by using a simulated annealing algorithm. The fitted rates included glutamatergic TCA cycle ($V_{tca(Glu)}$), GABA shunt (V_{shunt}), net GABAergic TCA cycle flux ($V_{TCA(GABA)Net}$), astroglial TCA cycle ($V_{tca(A)}$), and exchange rate between α-ketoglutarate-glutamate (V_x) and different dilution fluxes.

Statistics

The Data Analysis Tool package of Microsoft Excel 2007 was used for the Statistical analysis. Analysis of variance (ANOVA) analysis was carried out to determine the significance of differences in amino acids labeling between AβPP-PS1 and wild-type mice within same brain region. One-way ANOVA was carried out to find the significance of differences in the concentrations and metabolic rates among different groups. The post hoc Tukey honest test was performed to identify the significance of difference between groups.

Results

Learning and memory in AβPP-PS1 mice

Learning and memory in mice were assessed using MWM test. Wild type (WT) mice showed a good learning pattern during four days of training but AβPP-PS1 mice could not locate the platform even after four days of intense training (Figure 2(a)). Memory tests carried out two days after the training, revealed that WT mice had good memory retention, and could locate the platform in 47 ± 11 s. In contrast, the escape latency in AβPP-PS1 mice was more than 90 s suggesting impaired memory in AD mice (Figure 2(b)).

Level of neurochemicals in AβPP-PS1

Neurochemical profile obtained using *ex vivo* ^{1}H NMR spectroscopy in different regions of brain indicated that the levels of neurometabolites were significantly perturbed in AβPP-PS1 mice when compared with age-matched WT controls. The levels of glutamate and

Table 1. Percent ^{13}C labeling of brain amino acids from [2-^{13}C]acetate in AβPP-PS1 and wild-type (WT) mice.

Brain region	Infusion time (min)	Groups	Amino acids					$CMR_{Ac(ox)}$ (μmol/g/min)	$V_{cyc}/V_{TCA(N)}$	
			Glu_{C4}	$GABA_{C2}$	Gln_{C4}	Asp_{C3}	Glu_{C3}		Glu'ergic	GABAergic
Cortex	15	WT	3.8 ± 0.2	3.2 ± 0.7	10.4 ± 0.8	2.3 ± 0.2	0.9 ± 0.2	0.051 ± 0.005	–	–
		AβPP-PSI	3.9 ± 0.1	3.4 ± 0.9	11.9 ± 1.4	2.4 ± 0.5	0.9 ± 0.2	0.064 ± 0.007*	–	–
	90	WT	8.3 ± 0.8	7.4 ± 1.0	17.0 ± 1.2	6.9 ± 0.6	7.6 ± 2.4	–	0.43 ± 0.14	0.51 ± 0.14
		AβPP-PSI	9.3 ± 2.2	7.7 ± 1.8	19.0 ± 3.0	7.4 ± 2.8	6.5 ± 3.7	–	0.44 ± 0.06	0.60 ± 0.08
Hippocampus	15	WT	3.9 ± 0.3	2.4 ± 0.4	12.5 ± 1.0	ND	ND	0.051 ± 0.003	–	–
		AβPP-PSI	3.7 ± 0.4	2.2 ± 0.8	13.2 ± 0.5	ND	ND	0.056 ± 0.004*	–	–
	90	WT	7.3 ± 1.6	6.8 ± 1.7	16.3 ± 2.1	ND	ND	–	0.39 ± 0.14	0.50 ± 0.11
		AβPP-PSI	7.6 ± 0.9	6.8 ± 0.7	17.7 ± 0.9	ND	ND	–	0.48 ± 0.13	0.64 ± 0.16
Striatum	15	WT	4.2 ± 0.1	2.2 ± 0.1	12.2 ± 1.3	ND	ND	0.051 ± 0.007	–	–
		AβPP-PSI	3.5 ± 0.7	1.5 ± 0.4	10.7 ± 1.6	ND	ND	0.051 ± 0.003	–	–
	90	WT	7.5 ± 1.7	6.2 ± 1.6	15.5 ± 3.2	ND	ND	–	0.38 ± 0.04	0.46 ± 0.12
		AβPP-PSI	8.7 ± 2.0	7.3 ± 2.1	18.6 ± 3.3	ND	ND	–	0.44 ± 0.06	0.49 ± 0.08

ND: not determined. Mice were administered [2-^{13}C]acetate for 15 and 90 min. The ^{13}C labeling of amino acids was measured in brain tissue extracts using ^{1}H-[^{13}C]-NMR spectroscopy. $CMR_{Ac(ox)}$ and $V_{cyc}/V_{TCA(N)}$ were calculated using equations (1) to (3). Values represent mean ± SEM.
*$p < 0.05$ when compared with respective controls.

aspartate were significantly ($p < 0.05$) lower in hippocampal and cortical regions in AβPP-PS1 mice (Table S1). Additionally, the level of *N*-acetyl-aspartate (NAA) was found to be decreased in hippocampal (AβPP-PS1 6.6 ± 0.2 μmol/g; WT 7.6 ± 0.2 μmol/g, $p < 0.01$) and cortical (AβPP-PS1 7.0 ± 0.1 μmol/g; WT 7.5 ± 0.2 μmol/g, $p < 0.01$) regions in AβPP-PS1 mice. Interestingly, there was significant increase in the level of myo-inositol in hippocampal (WT 7.3 ± 0.2 μmol/g; AβPP-PS1 8.5 ± 0.2 μmol/g, $p < 0.01$) and cortical (AβPP-PS1 7.8 ± 0.2 μmol/g; WT 7.2 ± 0.2 μmol/g, $p < 0.01$) regions in AβPP-PS1 mice. There were no significant changes in the levels of other metabolites in different brain regions in AβPP-PS1 mice (Supplementary Table S1).

Astroglial activity in AβPP-PS1 mice

The astroglial metabolic activity was measured by following the ^{13}C labeling of cerebral amino acids from a 15-min infusion of [2-^{13}C]acetate in mice (Figure 3(a)). The concentration of Gln_{C4} was found to be increased in the hippocampal (0.65 ± 0.06 vs. 0.57 ± 0.03 μmol/g, $p < 0.01$) and cortical (0.71 ± 0.08 vs. 0.54 ± 0.05 μmol/g, $p < 0.01$) regions in AβPP-PS1 mice when compared with WT controls. The striatal region did not exhibit significant change in the Gln_{C4} labeling from [2-^{13}C]acetate (0.57 ± 0.04 vs. 0.55 ± 0.08, $p > 0.05$). The increased ^{13}C labeling of Gln_{C4} from [2-^{13}C]acetate indicates enhanced astroglial metabolic activity in the hippocampus and cerebral cortex of AβPP-PS1 mice (Figure 3(b), Table 1).

Ratio V_{cyc}/V_{tca} in AβPP-PS1 mice

For the measurement of ratio of neurotransmitter cycle to TCA cycle flux, an infusion of [2-^{13}C]acetate was carried out in mice for 90 min so that ^{13}C labeling of brain amino acids have attained an isotopic steady state. No significant change ($p > 0.1$) in the steady state labeling of Gln_{C4}, Glu_{C4} and $GABA_{C2}$ from [2-^{13}C]acetate was observed between AβPP-PS1 and control mice (Table 1). The ratio of neurotransmitter cycle flux to corresponding TCA cycle of different neurons was calculated using equations (2) and (3), respectively. The ratios, $V_{cyc(Glu\text{-}Gln)}/V_{TCA(Glu)}$ and $V_{cyc(GABA\text{-}Gln)}/V_{TCA(GABA)}$, in AβPP-PS1 mice were not significantly ($p > 0.16$) different when compared with controls (Table 1).

Labeling of brain amino acids from [1,6-$^{13}C_2$]glucose

To derive the ^{13}C turnover of brain amino acids, [1,6-$^{13}C_2$]glucose was infused for different time points ranging from 10 to 90 min, and percent ^{13}C enrichment of brain amino acids was measured in tissue extracts using ^{1}H-[^{13}C]-NMR spectroscopy. The ^{1}H-[^{13}C]-NMR spectral time course depicting the ^{13}C labeling of hippocampal metabolites in control mice is presented in Figure 4(a). The ^{13}C labeled Glu_{C4} and $GABA_{C2}$ could be seen at the early infusion time (10 min). Additionally, resonances from Glu_{C3}, Asp_{C3}, $GABA_{C3}$, and $GABA_{C4}$ which are labeled in the second turn of TCA cycle could be seen in the spectra recorded at 30 min onward. A similar pattern was seen for the AβPP-PS1 mice (Figure 4(b)). However, the intensity of ^{13}C labeled signal at earlier time points (10 and 30 min) is lower in AβPP-PS1 mice when compared with controls, suggesting a slower turnover of metabolites in transgenic mice (Figure 4). The ^{13}C turnover curves of amino acids from [1,6-$^{13}C_2$]glucose were created by plotting the percent ^{13}C labeling of amino acids with time (Figure 5), and were used for metabolic flux analysis.

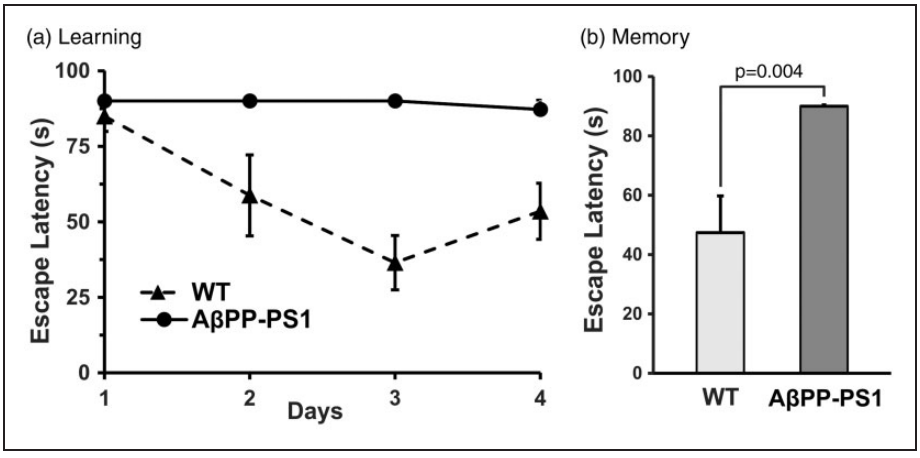

Figure 2. Learning and memory in AβPP-PS1 and control mice. Learning and memory were evaluated using Morris Water Maze test. (a) Learning curve of AβPP-PS1 and wild type mice during training period. (b) The memory of AβPP-PS1 and control mice: The escape latency of mice to reach the platform was evaluated on the seventh day.

Glutamatergic and GABAergic fluxes in AβPP-PS1 mice brain

The metabolic fluxes associated with glutamatergic and GABAergic neurons were obtained by analysis of ^{13}C labeling of amino acids from [1,6-$^{13}C_2$]glucose. The best fit of the metabolic model to the hippocampus data is depicted in Figure 5. The rates of neuronal glucose oxidation ($CMR_{Glc(Ox)}$) and neurotransmitter cycle (V_{cyc}) thus obtained in different brain regions in AβPP-PS1 and age-matched controls are presented in Figure 6.

Hippocampus. The cerebral metabolic rates of neuronal glucose oxidation (CMR_{Glc}) and neurotransmitter cycle was significantly lower ($p < 0.01$) in the hippocampus of AβPP-PS1 mice when compared with WT controls (Figure 6). The rate of glucose oxidation by glutamatergic neurons ($CMR_{Glc(Glu)}$) was found to be

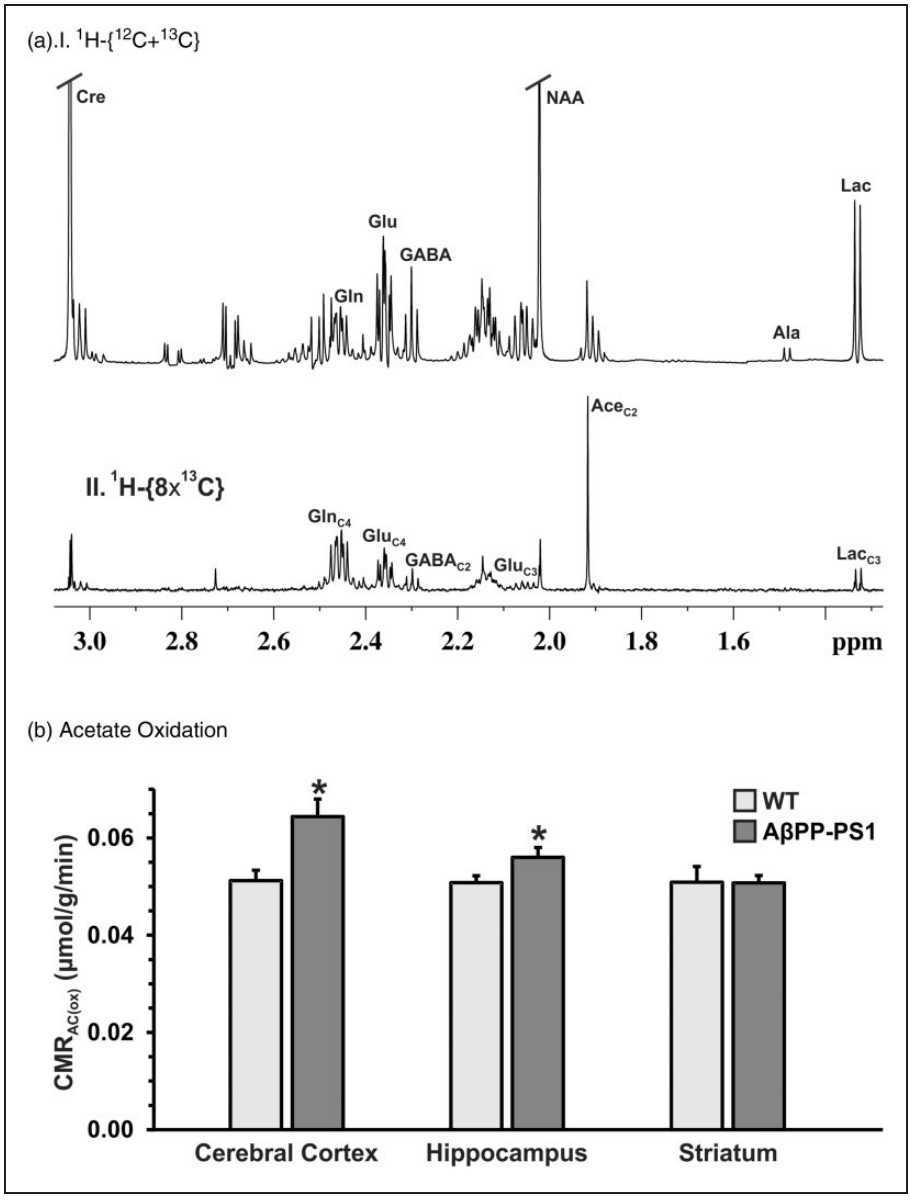

Figure 3. (a) ^{1}H-[^{13}C]-NMR spectrum depicting ^{13}C labeling of hippocampal amino acids from [2-^{13}C]acetate in AβPP-PS1 mice. Mice were infused with [2-^{13}C]acetate for 15 min. Metabolites were extracted from frozen hippocampal tissue. ^{1}H-[^{13}C]-NMR spectra were recorded in hippocampal extracts. (b) The cerebral metabolic rate of acetate oxidation ($CMR_{Ac(ox)}$) in AβPP-PS1 and control mice. The ^{13}C labeling of brain amino acids were measured using ^{1}H-[^{13}C]-NMR spectroscopy in tissue extracts. The $CMR_{Ac(ox)}$ was calculated using equation (1).

*$p < 0.5$ when compared with the respective controls.

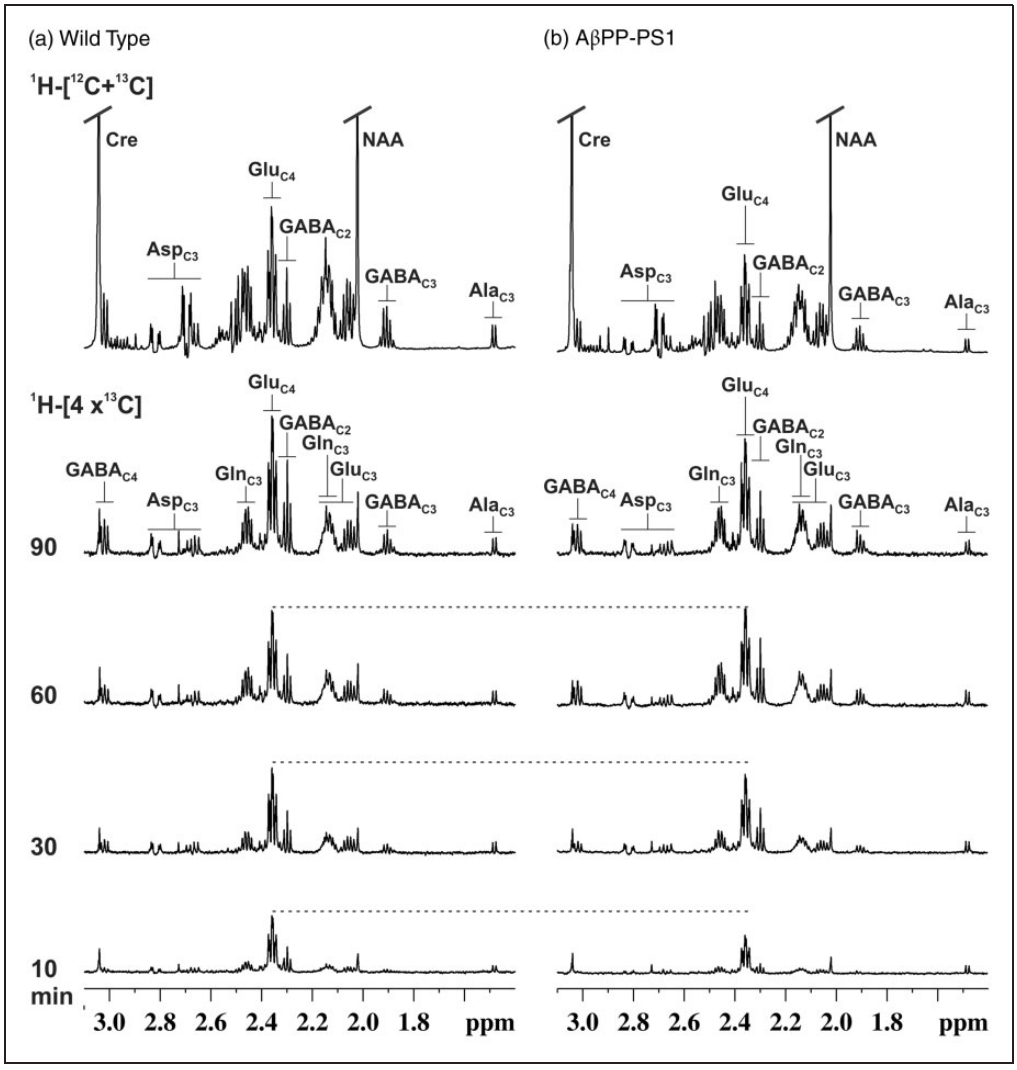

Figure 4. Representative ^{1}H-[^{13}C]-NMR spectra of hippocampal tissue extracts in (a) Wild type, and (b) AβPP-PS1 mice. [1,6-$^{13}C_2$]Glucose was administered in mice for pre-defined time, and ^{1}H-[^{13}C]-NMR spectra were recorded from hippocampal tissue extracts. The top spectrum was used for the quantification of concentrations of metabolites, while lower spectra (^{1}H-[4x^{13}C]) were used to determine the ^{13}C turnover of brain amino acids. Peaks labeling are: Ala_{C3}, alanine-C3; Asp_{C3}, asparate-C3; $GABA_{C2}$, GABA-C2; Gln_{C4}, glutamine-C4; Glu_{C4}, glutamate-C4.

reduced significantly ($p < 0.001$) in hippocampus (0.148 ± 0.003 μmol/g/min) of AβPP-PS1 mice when compared with controls (0.255 ± 0.005 μmol/g/min) (Figure 6(a)II). Likewise, the glutamate–glutamine neurotransmitter cycling flux was found to be reduced in AβPP-PS1 mice (control: 0.245 ± 0.005; AβPP-PS1: 0.118 ± 0.002 μmol/g/min, $p < 0.001$) (Figure 6(b)II). The rate of glucose oxidation by GABAergic neurons ($CMR_{Glc(GABA)}$) was found to be reduced by 17% (0.086 ± 0.002 vs. 0.106 ± 0.002 μmol/g/min, $p < 0.001$) (Figure 6(a)III). Similar to glutamatergic neurotransmission, the GABA-glutamine neurotransmitter cycle flux was found to be decreased in AβPP-PS1 mice (0.090 ± 0.002 vs. 0.135 ± 0.003 mol/g/min, $p < 0.001$) (Figure 6(b)III).

Cerebral cortex. The $CMR_{Glc(Glu)}$ was found to be reduced by 36% (control: 0.346 ± 0.007; AβPP-PS1: 0.223 ± 0.002 μmol/g/min, $p < 0.001$), while $CMR_{Glc(GABA)}$ exhibited a reduction of only 18% (control 0.110 ± 0.002; AβPP-PS1 0.090 ± 0.002 μmol/g/min, $p < 0.01$). Additionally, the rates of glutamate–glutamine (0.191 ± 0.002 vs. 0.305 ± 0.003 μmol/g/min) and GABA-glutamine (0.097 ± 0.001 vs. 0.132 ± 0.002 μmol/g/min) were reduced significantly in AβPP-PS1 mice when compared with WT controls (Figure 6(b)II/III).

Striatum. Similar to the hippocampus and cerebral cortex, the $CMR_{Glc(ox)}$ of glutamatergic neurons was found to be decreased in the striatum of AβPP-PS1

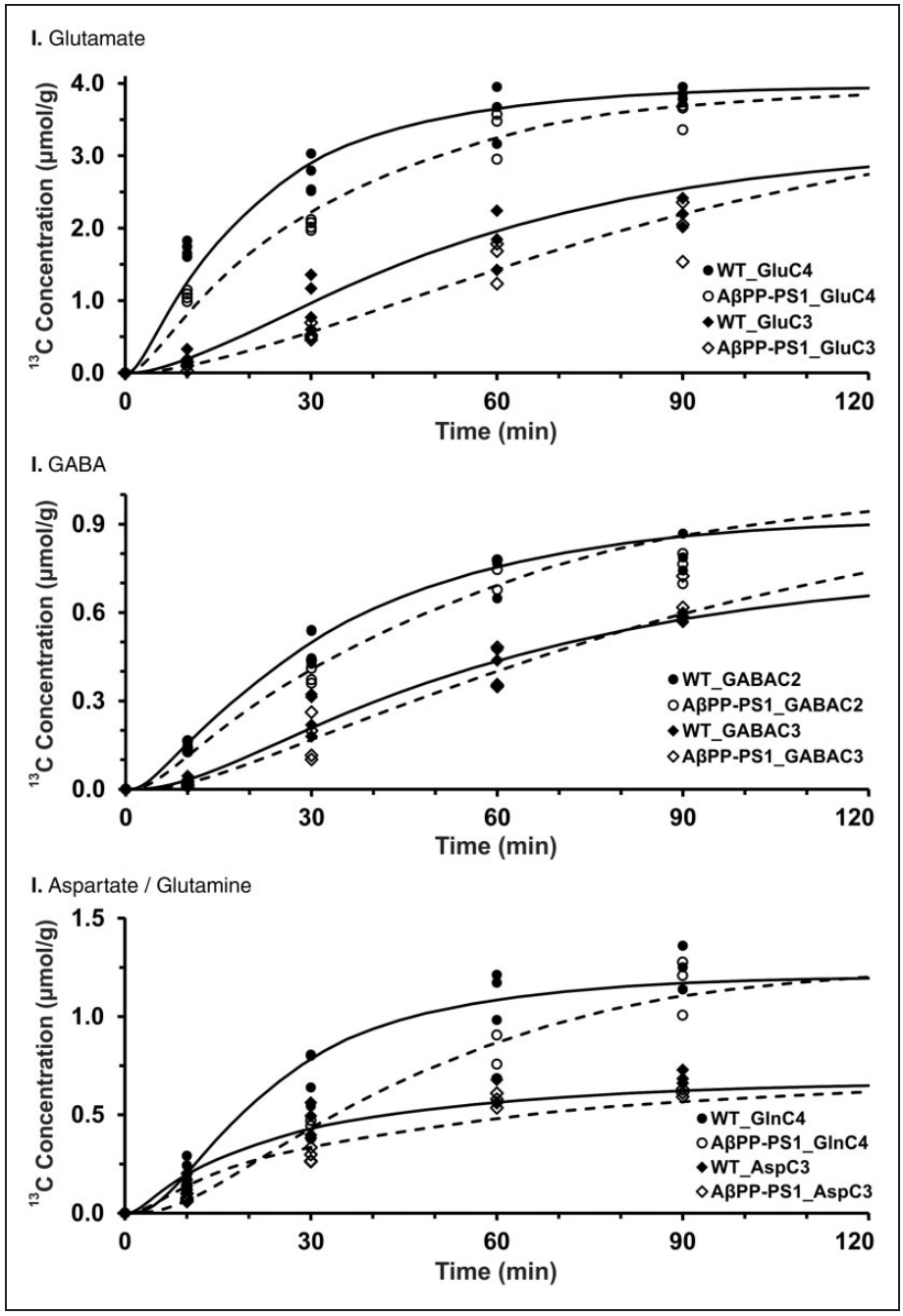

Figure 5. Fit of a three-compartment metabolic model to ^{13}C turnover of hippocampal amino acids in (I) glutamate, (II) GABA, and (III) glutamine/aspartate. [1,6-$^{13}C_2$]Glucose was administered in mice for pre-defined time. ^{13}C concentrations of amino acids were measured in hippocampal extracts in ^{1}H-[^{13}C]-NMR spectra. Symbols depict to the measured labeling, while lines represent the best fit of the metabolic model to the measured values.

mice (0.173 ± 0.002, $p < 0.01$, -23%) when compared with WT controls (0.224 ± 0.006 µmol/g/min). The glutamate–glutamine neurotransmitter cycle rate was also found to be reduced (-33%) in AβPP-PS1 mice (0.132 ± 0.002 vs. 0.197 ± 0.004 µmol/g/min). Similarly, $CMR_{Glc(GABA)}$ was reduced (-36%) in AβPP-PS1 (0.063 ± 0.001 vs. 0.099 ± 0.002 µmol/g/min) as compared with controls (Figure 6(a)III). Moreover, GABA-glutamine neurotransmitter cycle flux was reduced (-33%) in AβPP-PS1 (0.065 ± 0.001 µmol/g/min) mice when compared with age matched controls (0.097 ± 0.002 µmol/g/min) (Figure 6(b)III).

These data indicate that AβPP-PS1 mice exhibit decreased excitatory and inhibitory neurotransmission

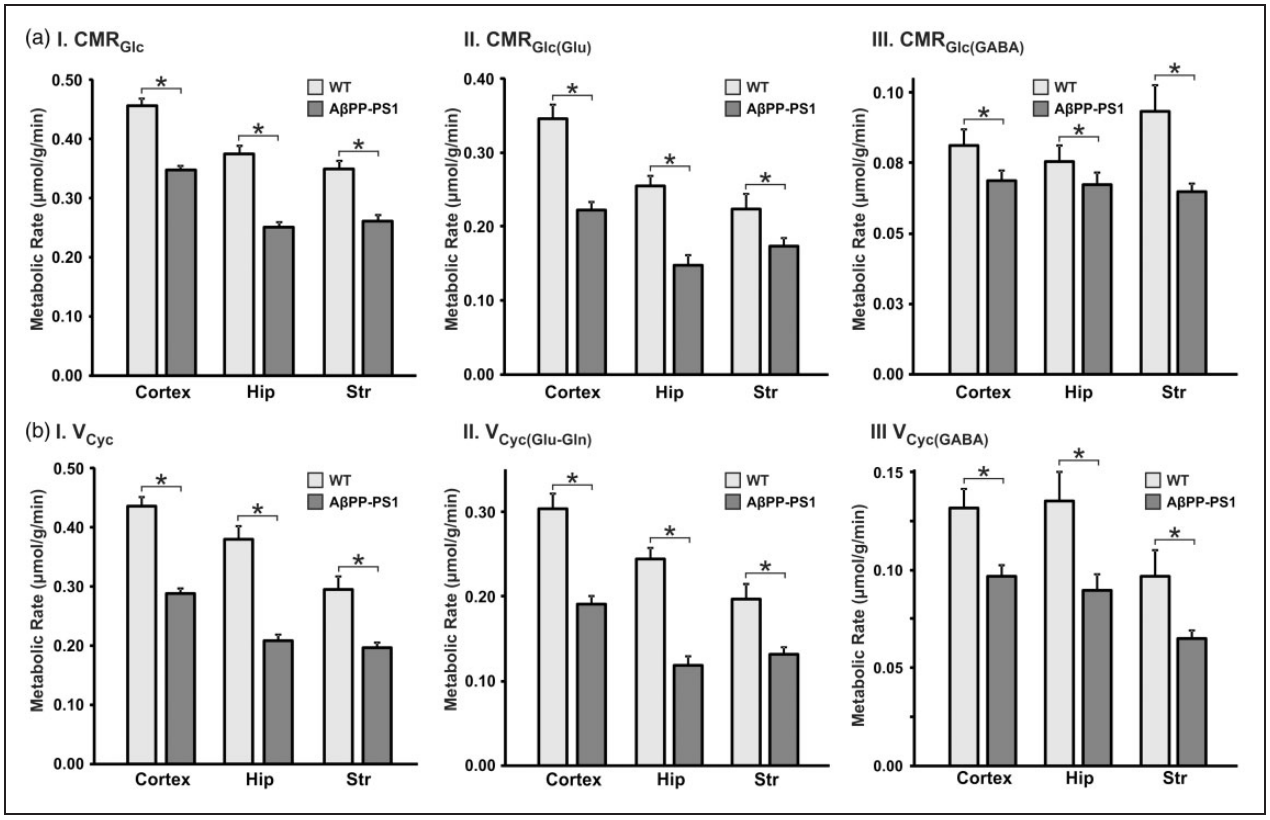

Figure 6. Metabolic rates in AβPP-PS1 and WT mice. (a.I) Cerebral metabolic rate of glucose oxidation; (a.II) Rate of glucose oxidation in glutamatergic neurons; (a.III) rate of glucose oxidation in GABAergic TCA cycle; (b.I) neurotransmitter cycle; (b.II) glutamate-glutamine cycle; (b.III) GABA-glutamine cycle. Metabolic rates were determined by fitting a three compartment model to the measured ^{13}C turnover of amino acids from [1,6-$^{13}C_2$]glucose. Values represent mean ± SEM. *$p < 0.001$.

across brain. It is noteworthy that reduction in glutamatergic fluxes was higher than GABAergic rates.

Discussion

The quantitative significance of brain energy metabolism in AD has not been explored. Present study evaluates for the first time, the excitatory and inhibitory neurotransmitter cycling flux, and energy demand of different neural cell types (neurons and astroglia) by using a three compartment metabolic model across brain at the stage of high plaque loading in AβPP-PS1 mice. Our analysis indicates that astroglial activity is increased while neuronal function is decreased in AD mice.

The current study involved the use of AβPP-PS1 mice for investigation of neuronal and astroglial metabolic rates in AD. The plaque pathology, memory and neurotransmission have been studied in details in these mice. There was no detectable plaque pathology observed in hippocampus at five months of age.[22] There was no impairment in conditional learning in these mice at the age of five months. The electrophysiological studies have suggested impaired neuronal activity in these mice. The whole-cell patch clamp recording of CA3 neurons in AβPP-PS1 mice at the age of six months indicated reduction in the amplitude of excitatory post synaptic currents associated with glutamatergic neurons.[23] Moreover, the long-term potentiation of excitatory post synaptic currents of α-amino-3-hydroxy-5-methyl-4-isoxazolepropionic acid (AMPA) receptor was absent in AβPP-PS1 mice, further suggesting impairment of neurotransmission in these mice. The amyloid deposition was clearly visible in AβPP-PS1 mice during the age 6–9 months,[24] and increased severely beyond 12 months. Moreover, our immunohistological examination using Aβ-antibody has suggested huge burden of plaques in the cerebral cortex and hippocampus in AβPP-PS1 mice at the age of 12 months (Supplementary Figure S1). The memory analysis using different paradigms has shown impairment in learning and memory at and beyond six months of age in AβPP-PS1 mice.[25] Our analysis using MWM paradigm has also indicated reduction in the learning and memory in AβPP-PS1 mice at the age of 12 months. The ^1H MRS analysis of neurochemical profile has indicated a reduction in the levels of *N*-acetyl aspartate and glutamate in these mice with advancing

age.[26] Moreover, an increase in the level of myo-inositol with age in AβPP-PS1 mice was also reported. These age-dependent changes in the levels of neurometabolites in AβPP-PS1 mice agree well with ^{1}H MRS studies in human AD. These findings suggest that AβPP-PS1 mice closely mimic the pathology of human AD condition.

Neurochemical homeostasis in AD brain

Neurochemical profile has been investigated under AD condition in human[27] as well as in animal models. These studies have shown reduction in level of NAA in different brain regions of AD patients.[28] A recent study has also indicated decreased glutamate level in AD patients.[27] Moreover, a reduction in the level of NAA has been reported at the age of 12 months in the hippocampus of AβPP-PS1 mice.[26] The findings of decreased level of glutamate and NAA in cortical and hippocampal regions of AβPP-PS1 in the current study are in good accordance with these reports. The reduction in NAA level in the cerebral cortex and hippocampus is suggestive of reduced neuronal viability and/or density in AD brain. Hippocampus is known to be responsible for contextual and declarative memory. Glutamate is linked with long-term potentiation and memory,[29] and NAA is considered to be the neuronal viability and density marker.[30] Hence, reduction in the number of glutamatergic neurons in the hippocampus may be a plausible cause for the loss in memory in AD subjects. The level of myo-inositol has been shown to increase with age in AβPP-PS1 mice.[26] Myo-inositol has been believed to be a glial marker.[31] Our findings of increased level of myo-inositol in the cerebral cortex and hippocampus of AβPP-PS1 mice suggest gliosis like condition in the AD brain.

Neuronal and astroglial metabolic activity in AD

There are conflicting reports about cerebral metabolism in rodent models of AD. The ^{13}C labeling of brain amino acids were reported to increase in three-month old P301L mice[32] and in seven-month old triple transgenic mice suggesting hyper metabolic state at early stage of AD.[33] However, metabolic analysis conducted at later age (13 months) suggested hypo-metabolism in triple transgenic mice.[34] Our earlier measurements in AβPP-PS1 at pre-symptomatic stage (6 months) has revealed decreased metabolic rates of excitatory and inhibitory neurons.[6] The data reported from the current study suggest the neuronal hypo-metabolism observed at pre-symptomatic stage persist at the stage of high plaque loading in AβPP-PS1 mice.

Traditionally, glucose metabolism in human subject has been measured using positron emission tomography in conjunction with administration of ^{18}F-labeled fluorodeoxyglucose. This approach provides information about glucose phosphorylation / consumption in brain. A widespread reduction in local cerebral glucose consumption has been reported in the posterior cingulated, lateral temporo-parietal, and occipital cortices of AD patients.[35] Additionally, hypo-glucose metabolism has also been observed in the posterior cingulate and temporo-parietal regions in mild cognitive impaired subjects.[36] The cerebral metabolic rate of glucose utilization (CMR_{Glc}) in the current study was found to be decreased in the hippocampus (−37%), cerebral cortex (−23%), and striatum (−29%) in AβPP-PS1 mice, and agrees very well with human AD studies. Analysis of pyruvate dehydrogenase flux at the cellular level suggested that the hypo-metabolism of glucose in AβPP-PS1 mice brain is due to reduced activity of both glutamatergic and GABAergic neurons across brain.

The stochiometric coupling between neuronal glucose oxidation and neurotransmitter cycling has been well established in healthy brain.[9,10] Qualitative analysis of energy metabolism in mouse model of AD[6,34] has shown a reduction in the labeling of $Glu_{C4/C3}$, $GABA_{C2/C3}$, and $Gln_{C4/C3}$ labeling from [1-^{13}C]glucose/[1,6-$^{13}C_2$]glucose. These studies suggest that coupling between neurotransmitter cycling and neuronal glucose oxidation is also maintained under disease conditions. The findings of current study indicate that the flux through neurotransmitter and neuronal glucose oxidation are coupled in AD. Therefore, measurement of neuronal glucose oxidation may be used to assess the neurotransmitter cycling under various neurological conditions.

The reactive microglia are shown to be enhanced in AβPP-PS1 mice.[37] Moreover, the degree of microglial activation increases with AD severity, and with Aβ plaque load.[38] Though glia have been associated with neuro-inflammation, there is no quantitative report pertaining to the glial metabolic activity in AD condition. Acetate is specifically metabolized in astrocytes because monocarboxylate transporters, which are used to transport acetate from blood to brain, are exclusively localized on glial cells.[19] Therefore, acetate has been used extensively to explore the astroglial metabolic activity in different neurological conditions.[39] The astroglial activity was reported to be un-perturbed in a triple transgenic mouse model of AD,[33] while it was reduced in rat model.[40] Our findings of increased oxidation of acetate in cortical and hippocampal region in AβPP-PS1 mice as compared with controls (Figure 3(b)) suggest that the astroglial activity is increased in AD.

The astrolglial metabolic activity is used to sustain different cellular processes such as efflux of Na^{+} that is co-transported with glutamate into astrocytes, pyruvate carboxylation, and conversion of glutamate (plus GABA) to glutamine. Moreover, astrogliosis has

been implicated in neuro-inflammatory condition. The observed metabolic activity of astroglia indicates the sum total of energy requirements of above mentioned fluxes. The pyruvate carboxylation has been shown to be reduced in AβPP-PS1 mice at the age of 20 months.[41] Therefore, the observed increase in astroglial activity measured using [2-^{13}C]acetate in the current study suggests the dominance of neuro-inflammation over other two pathways (glutamine synthesis and pyruvate carboxylation) in AD condition.

Excitatory and inhibitory neurotransmission in AD

Glutamate, the major excitatory neurotransmitter in the central nervous system, is involved in learning, memory, and cognition. Though level of glutamate has been reported to be lower in the cerebral cortex and hippocampus in transgenic models of AD in mice,[26,40] there is no quantitative information pertaining to flux associated with trafficking of glutamate between neuron and astrocytes, commonly known as neurotransmitter cycling, is available. A recent study conducted in transgenic rat model of AD has shown small reduction in ^{13}C labeling of glutamate and GABA in hippocampus while cortical region was unperturbed.[42] Additionally, the ^{13}C labeling of amino acids in whole brain extract was shown to be decreased in a triple transgenic mouse model of AD.[34] These studies qualitatively suggested hypo-metabolism and reduced neurotransmitter cycling in AD condition. Our findings suggest that excitatory activity associated with glutamatergic neurons are severely impaired in hippocampus followed by cerebral cortex and striatum, while the inhibitory activity comprising of GABAergic neurons is decreased highest in the striatum, suggesting differential perturbations in excitatory and inhibitory neurotransmission in AD brain. The severe impairment in glutamatergic neurotransmission across brain points towards reduced firing of excitatory neurons in AD. Since synaptic transmission associated with glutamatergic neurons is implicated in long-term potentiation and memory,[29] the reduction in glutamatergic neurotransmission in hippocampus explains loss of memory in AD patients.

Relevance of neurometabolic measurement in diagnosis of AD

Our analysis in AβPP-PS1 mice at the age of six month has indicated no significant perturbation in neurometabolites homeostasis. However, reduction in the ^{13}C labeling of amino acids in the cerebral cortex and hippocampus from labeled glucose has suggested severe reduction in neurotransmitter energy metabolism at pre-symptomatic stage of AD.[6] The finding from present study revealed that neurometabolites homeostasis in AβPP-PS1 mice is perturbed in the cerebral cortex and hippocampus at stage of high plaque loading. Additionally, findings of reduction in glutamatergic and GABAergic neurometabolic activity indicates decreased neurotransmission at the pre-symptomatic stage as well as at the high plaque loading. Interestingly, astroglial metabolic activity that was unperturbed at pre-symptomatic stage was found to be increased in AβPP-PS1 mice at the stage of high plaque loading. These data point towards differential perturbation of neural metabolic activity with the progress of AD, which may be useful for better understanding of different stages of disease.

Summary

^{1}H-NMR analysis revealed perturbation in homeostasis of neurometabolites across brain. Levels of glutamate and NAA are reduced in cortical and hippocampal regions, while no change was noted in striatal region. Interestingly, neuronal glucose oxidation and neurotransmitter cycling flux of glutamatergic and GABAergic neurons were found to be impaired across brain in AβPP-PS1 mice. In contrast, the astroglial metabolic rate was increased in the cerebral cortex and hippocampus in AD mice. Previous study in AD mice at pre-symptomatic stage has indicated impairment of neuronal metabolic activity without any perturbation in neurometabolite homeostasis.[6] Therefore, analysis of neuronal and astroglial metabolic rates in addition to levels of neurometabolites would provide a comprehensive status of brain functions, which have potential for specific diagnosis of AD.

Funding

The author(s) received no financial support for the research, authorship, and/or publication of this article.

Acknowledgments

We thank Dr Robin A de Graff, Yale University for providing the ^{1}H-[^{13}C]-NMR pulse sequence, Mr Jedy Jose for breeding mice, and Mr Bhargidhar Babu for assistance in animal studies, Dr Swati Maitra for help in carrying out MWM experiments. Authors would like to thank Prof. Subhash C Lakhotia, Banaras Hindu University for the critical review and suggestions for the manuscript. The Behavioral facility is dully acknowledged for MWM test. All NMR experiments were performed at NMR Microimaging and Spectroscopy Facility, CCMB, Hyderabad, India. This study was supported by grants from the Department of Biotechnology (BT/PR14064/Med/30/359/2010), Department of Science and Technology (CO/AB/013/2013), and CSIR network project BSC0208.

Declaration of conflicting interests

The author(s) declared no potential conflicts of interest with respect to the research, authorship, and/or publication of this article.

Authors' contributions

ABP designed research; VT and PV performed research; ABP, VT, and KS analyzed data; ABP and KS prepared figures; ABP and VT interpreted the data; ABP, VT, and KS wrote the paper; and ABP supervised and directed the overall project. All authors reviewed the manuscript.

Supplementary material

Supplementary material for this paper can be found at the journal website: http://journals.sagepub.com/home/jcb

References

1. Goedert M and Spillantini MG. A century of Alzheimer's disease. *Science* 2006; 314: 777–781.
2. Delacourte A, David JP, Sergeant N, et al. The biochemical pathway of neurofibrillary degeneration in aging and Alzheimer's disease. *Neurology* 1999; 52: 1158–1165.
3. Hardy J and Selkoe DJ. The amyloid hypothesis of Alzheimer's disease: progress and problems on the road to therapeutics. *Science* 2002; 297: 353–356.
4. DeFelipe J and Farinas I. The pyramidal neuron of the cerebral cortex: morphological and chemical characteristics of the synaptic inputs. *Prog Neurobiol* 1992; 39: 563–607.
5. Rabinovici GD, Furst AJ, Alkalay A, et al. Increased metabolic vulnerability in early-onset Alzheimer's disease is not related to amyloid burden. *Brain* 2010; 133: 512–528.
6. Tiwari V and Patel AB. Impaired glutamatergic and GABAergic function at early age in AβPPswe-PS1dE9 mice: implications for Alzheimer's disease. *J Alzheimer's Dis JAD* 2012; 28: 765–769.
7. Mattson MP and Kater SB. Excitatory and inhibitory neurotransmitters in the generation and degeneration of hippocampal neuroarchitecture. *Brain Res* 1989; 478: 337–348.
8. Ottersen OP and Storm-Mathisen J. Excitatory amino acid pathways in the brain. *Adv Exp Med Biol* 1986; 203: 263–284.
9. Patel AB, de Graaf RA, Mason GF, et al. Glutamatergic neurotransmission and neuronal glucose oxidation are coupled during intense neuronal activation. *J Cereb Blood Flow Metab* 2004; 24: 972–985.
10. Sibson NR, Dhankhar A, Mason GF, et al. Stoichiometric coupling of brain glucose metabolism and glutamatergic neuronal activity. *Proc Natl Acad Sci U S A* 1998; 95: 316–321.
11. Rothman DL, Behar KL, Hyder F, et al. In vivo NMR studies of the glutamate neurotransmitter flux and neuroenergetics: implications for brain function. *Annu Rev Physiol* 2003; 65: 401–427.
12. Jankowsky JL, Fadale DJ, Anderson J, et al. Mutant presenilins specifically elevate the levels of the 42 residue beta-amyloid peptide in vivo: evidence for augmentation of a 42-specific gamma secretase. *Hum Mol Genet* 2004; 13: 159–170.
13. Vorhees CV and Williams MT. Morris water maze: procedures for assessing spatial and related forms of learning and memory. *Nat Protoc* 2006; 1: 848–858.
14. Tiwari V, Ambadipudi S and Patel AB. Glutamatergic and GABAergic TCA cycle and neurotransmitter cycling fluxes in different regions of mouse brain. *J Cereb Blood Flow Metab* 2013; 33: 1523–1531.
15. Patel AB, de Graaf RA, Rothman DL, et al. Evaluation of cerebral acetate transport and metabolic rates in the rat brain *in vivo* using ^{1}H-[^{13}C]-NMR. *J Cereb Blood Flow Metab* 2010; 30: 1200–1213.
16. Patel AB, Rothman DL, Cline GW, et al. Glutamine is the major precursor for GABA synthesis in rat neocortex in vivo following acute GABA-transaminase inhibition. *Brain Res* 2001; 919: 207–220.
17. Patel AB, de Graaf RA, Mason GF, et al. The contribution of GABA to glutamate/glutamine cycling and energy metabolism in the rat cortex in vivo. *Proc Natl Acad Sci U S A* 2005; 102: 5588–5593.
18. de Graaf RA, Brown PB, Mason GF, et al. Detection of [1,6-$^{13}C_2$]-glucose metabolism in rat brain by in vivo ^{1}H-[^{13}C]-NMR spectroscopy. *Magn Reson Med* 2003; 49: 37–46.
19. Waniewski RA and Martin DL. Preferential utilization of acetate by astrocytes is attributable to transport. *J Neurosci* 1998; 18: 5225–5233.
20. Mason GF and Rothman DL. Basic principles of metabolic modeling of NMR ^{13}C isotopic turnover to determine rates of brain metabolism in vivo. *Metab Eng* 2004; 6: 75–84.
21. Alcolea A, Carrera J and Medina A. A hybrid marquadrt-simulated annealing method for solving the groundwater inverse problem. Calibration and reliability in groundwater modeling. In: *Model-CARE 999 conference*, Zurich, Switzerland, September 1999, pp.157–163.
22. Dineley KT, Xia X, Bui D, et al. Accelerated plaque accumulation, associative learning deficits, and up-regulation of alpha 7 nicotinic receptor protein in transgenic mice co-expressing mutant human presenilin 1 and amyloid precursor proteins. *J Biol Chem* 2002; 277: 22768–22780.
23. Viana da Silva S, Haberl MG, Zhang P, et al. Early synaptic deficits in the APP/PS1 mouse model of Alzheimer's disease involve neuronal adenosine A2A receptors. *Nat Commun* 2016; 7: 11915.
24. Jankowsky JL, Fadale DJ, Anderson J, et al. Mutant presenilins specifically elevate the levels of the 42 residue beta-amyloid peptide in vivo: evidence for augmentation of a 42-specific gamma secretase. *Hum Mol Genet* 2004; 13: 159–170.
25. Wiesmann M, Jansen D, Zerbi V, et al. Improved spatial learning strategy and memory in aged Alzheimer AbetaPPswe/PS1dE9 mice on a multi-nutrient diet. *J Alzheimer's Dis JAD* 2013; 37: 233–245.
26. Marjanska M, Curran GL, Wengenack TM, et al. Monitoring disease progression in transgenic mouse models of Alzheimer's disease with proton magnetic

resonance spectroscopy. *Proc Natl Acad Sci U S A* 2005; 102: 11906–11910.
27. Rupsingh R, Borrie M, Smith M, et al. Reduced hippocampal glutamate in Alzheimer disease. *Neurobiol Aging* 2011; 32: 802–810.
28. Block W, Jessen F, Traber F, et al. Regional N-acetylaspartate reduction in the hippocampus detected with fast proton magnetic resonance spectroscopic imaging in patients with Alzheimer disease. *Arch Neurol* 2002; 59: 828–834.
29. Morris RG. Synaptic plasticity and learning: selective impairment of learning rats and blockade of long-term potentiation in vivo by the N-methyl-D-aspartate receptor antagonist AP5. *J Neurosci* 1989; 9: 3040–3057.
30. Adalsteinsson E, Sullivan EV, Kleinhans N, et al. Longitudinal decline of the neuronal marker N-acetyl aspartate in Alzheimer's disease. *Lancet* 2000; 355: 1696–1697.
31. Brand A, Richter-Landsberg C and Leibfritz D. Multinuclear NMR studies on the energy metabolism of glial and neuronal cells. *Dev Neurosci* 1993; 15: 289–298.
32. Nilsen LH, Rae C, Ittner LM, et al. Glutamate metabolism is impaired in transgenic mice with tau hyperphosphorylation. *J Cereb Blood Flow Metab* 2013; 33: 684–691.
33. Sancheti H, Patil I, Kanamori K, et al. Hypermetabolic state in the 7-month-old triple transgenic mouse model of Alzheimer's disease and the effect of lipoic acid: a ^{13}C-NMR study. *J Cereb Blood Flow Metab* 2014; 34: 1749–1760.
34. Sancheti H, Kanamori K, Patil I, et al. Reversal of metabolic deficits by lipoic acid in a triple transgenic mouse model of Alzheimer's disease: a ^{13}C NMR study. *J Cereb Blood Flow Metab* 2014; 34: 288–296.
35. Rabinovici GD, Rosen HJ, Alkalay A, et al. Amyloid vs FDG-PET in the differential diagnosis of AD and FTLD. *Neurology* 2011; 77: 2034–2042.
36. Drzezga A, Lautenschlager N, Siebner H, et al. Cerebral metabolic changes accompanying conversion of mild cognitive impairment into Alzheimer's disease: a PET follow-up study. *Eur J Nucl Med Mol Imaging* 2003; 30: 1104–1113.
37. Verkhratsky A, Olabarria M, Noristani HN, et al. Astrocytes in Alzheimer's disease. *Neurotherapeutics* 2010; 7: 399–412.
38. Griffin WS. Inflammation and neurodegenerative diseases. *Am J Clin Nutr* 2006; 83: 470S–474S.
39. Melo TM, Nehlig A and Sonnewald U. Metabolism is normal in astrocytes in chronically epileptic rats: a ^{13}C NMR study of neuronal-glial interactions in a model of temporal lobe epilepsy. *J Cereb Blood Flow Metab* 2005; 25: 1254–1264.
40. Nilsen LH, Melo TM, Saether O, et al. Altered neurochemical profile in the McGill-R-Thy1-APP rat model of Alzheimer's disease: a longitudinal in vivo ^{1}H MRS study. *J Neurochem* 2012; 123: 532–541.
41. Tiwari V and Patel AB. Pyruvate carboxylase and pentose phosphate fluxes are reduced in a betaPP-PS1 mouse model of Alzheimer's disease: a ^{13}C NMR study. *J Alzheimer's Dis* 2014; 41: 532–541.
42. Nilsen LH, Melo TM, Witter MP, et al. Early differences in dorsal hippocampal metabolite levels in males but not females in a transgenic rat model of Alzheimer's disease. *Neurochem Res* 2014; 39: 305–312.